Control of H_2 Dissociative Ionization in the Nonlinear Regime Using Vacuum Ultraviolet Free-Electron Laser Pulses

F. Holzmeier,[1,2,*] R. Y. Bello,[3,†] M. Hervé,[1] A. Achner,[4] T. M. Baumann,[4] M. Meyer,[4] P. Finetti,[5] M. Di Fraia,[5] D. Gauthier,[5,‡] E. Roussel,[5,§] O. Plekan,[5] R. Richter,[5] K. C. Prince,[5] C. Callegari,[5] H. Bachau,[6] A. Palacios,[3,7] F. Martín,[3,8,9] and D. Dowek[1]

[1]*Institut des Sciences Moléculaires d'Orsay CNRS, Université Paris-Sud, Université Paris-Saclay, 91405 Orsay Cedex, France*
[2]*Synchrotron SOLEIL, 91192 Gif-sur-Yvette, France*
[3]*Departamento de Química, Módulo 13, Universidad Autónoma de Madrid, 28049 Madrid, Spain*
[4]*European XFEL GmbH, 22869 Schenefeld, Germany*
[5]*Elettra-Sincrotrone Trieste, 34149 Basovizza, Trieste, Italy*
[6]*Centre des Lasers Intenses et Applications (UMR 5107 du CNRS-CEA-Université de Bordeaux), 351 Cours de la Libération, 33405 Talence cedex, France*
[7]*Institute for Advanced Research in Chemical Sciences (IAdChem), Universidad Autónoma de Madrid, 28049 Madrid, Spain*
[8]*Instituto Madrileño de Estudios Avanzados en Nanociencia (IMDEA-Nanociencia), Cantoblanco, 28049 Madrid, Spain*
[9]*Condensed Matter Physics Center (IFIMAC), Universidad Autónoma de Madrid, 28049 Madrid, Spain*

(Received 3 April 2018; published 7 September 2018)

The role of the nuclear degrees of freedom in nonlinear two-photon single ionization of H_2 molecules interacting with short and intense vacuum ultraviolet pulses is investigated, both experimentally and theoretically, by selecting single resonant vibronic intermediate neutral states. This high selectivity relies on the narrow bandwidth and tunability of the pulses generated at the FERMI free-electron laser. A sustained enhancement of dissociative ionization, which even exceeds nondissociative ionization, is observed and controlled as one selects progressively higher vibronic states. With the help of *ab initio* calculations for increasing pulse durations, the photoelectron and ion energy spectra obtained with velocity map imaging allow us to identify new photoionization pathways. With pulses of the order of 100 fs, the experiment probes a timescale that lies between that of ultrafast dynamical processes and that of steady state excitations.

DOI: 10.1103/PhysRevLett.121.103002

The control of molecular dissociation, i.e., chemical bond breaking, with vacuum and extreme ultraviolet radiation (VUV), is at the core of chemical reactivity and relies on the detailed understanding of the coupling between electronic and nuclear motion [1]. Such photo-induced fragmentation processes are of particular interest for large systems relevant for photochemical and biochemical applications [2,3]. However, in view of the complexity of dynamics in such systems, studies in small molecules, such as the H_2 benchmark (see [4] and references therein), are still required to understand and achieve quantum control of ultrafast molecular dynamics [5–7].

In the VUV, one-photon excitation of valence and inner-valence electrons commonly leads to single ionization of molecules. For such processes, nondissociative ionization (NDI) prevails, with a probability of dissociative ionization (DI) usually limited to a few percent [8]. In this context, recent time-dependent Schrödinger equation (TDSE) *ab initio* calculations of excitation and ionization of the H_2 molecule induced by few-femtosecond (fs) intense VUV laser pulses (10^{12} W/cm^2) predicted that the DI/NDI ratio can be increased by orders of magnitude due to resonance-enhanced two-photon ionization [9,10]. Considering all electronic and vibrational degrees of freedom (DOF) as well as electronic correlation, of particular importance in doubly excited states (DES) [11,12], they highlighted the key role of nuclear motion in the neutral excited molecule. Varying the pulse duration from 2 to 10 fs was proposed as a means to control the DI/NDI ratio.

Here, we choose an alternative strategy to investigate the role of the nuclear DOF in resonant two-VUV photon DI and NDI of H_2, taking advantage of the properties of the seeded free-electron laser (FEL) FERMI and its unique access to wavelengths up to 100 nm [13]. The parameter controlling the DI/NDI ratio consists of selecting single vibronic neutral intermediate states, here the H_2 ($B^1\Sigma_u^+$, v) manifold, relying on the high spectral resolution and precise tunability of the 100-fs pulses at FERMI [14] and on the brightness that allows for two-photon nonlinear ionization. Resonant excitation schemes involving single-pulse two-photon processes at FELs have mostly been applied to rare gases, highlighting the role of the resonance in the intermediate [15–17] or final state [18–20]. Studies of molecular dynamics were generally focused on non-resonant processes and characterized by recording ionic fragments [5,21,22].

For H_2, the excitation of rovibronic levels of the $B^1\Sigma_u^+$ state [23] was considered in resonant enhanced multiphoton ionization studies using nanosecond lasers. The molecular ionization continuum was mostly explored below the $H^+ + H$ dissociation threshold, where NDI competes with neutral dissociation (ND) involving the interaction of singly and doubly excited states of H_2 [24–27]. In such schemes, most H^+ products arise from subsequent photodissociation of the $H_2^+(X^2\Sigma_g^+)$ bound state or photoionization of $H(n)$ excited atoms produced by ND. ND and DI have also been investigated for continuum states reached by two-photon absorption from resonant $B^1\Sigma_u^+$ $(v = 5,\ J)$ rovibrational levels [28]. Dissociative two-photon above-threshold ionization was investigated using a high harmonic source [29].

In this work, the chosen two-photon VUV optical scheme produces resonant ionization in a region where H^+ ions can result only from DI. We demonstrate experimentally a remarkable enhancement and control of the DI/NDI ratio: This ratio can be even larger than unity, i.e., 2 orders of magnitude above one-photon ionization, and is controlled by selecting specific vibrational levels in the H_2 $(B^1\Sigma_u^+)$ intermediate state. Electron and ion velocity map imaging (VMI) allows for the identification of the DI and NDI mechanisms, and a comparison with *ab initio* calculations enlightens the dynamics at play within the 100-fs pulse duration.

Figure 1 illustrates the transition from the H_2 $(X^1\Sigma_g^+,\ v = 0)$ ground state into H_2 $(B^1\Sigma_g^+,\ v)$ states by the absorption of a VUV photon, followed by the absorption of a second photon into the $^1\Sigma_g^+$ continuum. For the $B^1\Sigma_u^+$ $(8 \le v \le 12)$ levels, corresponding to a favorable Franck Condon (FC) overlap with the $X^1\Sigma_g^+(v = 0)$ state, the vibrational spacing amounts to 130, 127, 123, and 119 meV, respectively. This relates to a 30–40 fs oscillation period. NDI populates exclusively the $H_2^+(1s\sigma_g\,^2\Sigma_g^+)$ ionic bound state, while DI may end up in the $H_2^+(2p\sigma_u\,^2\Sigma_u^+)$ channel as well. Depending on the selected vibrational level, different internuclear distances R are expected to contribute to the outcome of photoionization.

The experiment was performed at the low-density matter beam line of FERMI [30,31]. A supersonic jet of H_2 molecules was produced by expansion through a pulsed Even-Lavie valve. Small bandwidth [ca. 25 meV full width at half maximum (FWHM)] FEL pulses between 12.30 eV, the lowest photon energy accessible at FERMI, and 13 eV were produced at a 10 Hz repetition rate by tuning the six undulators of the FERMI FEL-1 setup [32] to the third harmonic of the seed laser. This bandwidth allows for the selection of single vibronic states comprising a few rotational levels. The desired tunability was obtained using an optical parametric amplifier laser system to provide seed pulses ranging from 280 to 365 nm. The 100–120 fs typical pulse length leads to VUV FEL pulses of 50–100 fs duration (FWHM) [14], which were focused

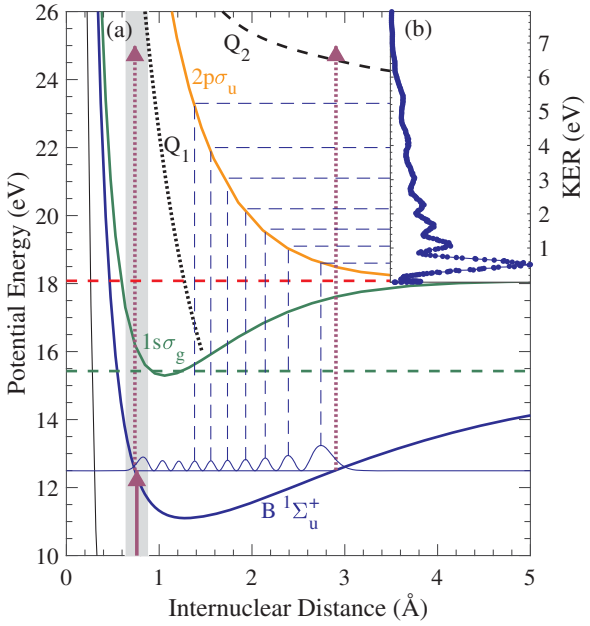

FIG. 1. (a) Schematic of resonant two-photon ionization via the $B^1\Sigma_u^+$ $(v = 9)$ neutral intermediate state (12.51 eV). Q_1 and Q_2 feature the lowest states of $^1\Sigma_g^+$ symmetry of each series of DES. The gray shaded area highlights the FC region for one-photon absorption from the $H_2(X^1\Sigma_g^+)$ ground state (solid arrow). The dashed arrows depict the range for absorption of the second photon after population of the $v = 9$ level. The dotted horizontal lines show the $H_2^+(^2\Sigma_g^+, v = 0)$ ionization threshold (green, 15.43 eV) and the $H^+ + H(1s)$ dissociation limit (red, 18.08 eV). Inset (b) depicts the measured KER spectrum for DI in resonance with the $B(v = 9)$ state.

by a Kirkpatrick-Baez optical system to a spot size of $30 \times 30\ \mu$m with a power density of 10^{12}–10^{13} W/cm^2. The light was linearly polarized perpendicular to the axis of the combined VMI and TOF spectrometer. Time-of-flight (TOF) mass spectra and photoelectron and fragment ion images were recorded at selected photon energies corresponding to excitation into vibrational levels of H_2^* bound neutral excited states. For the H^+ images, a gating scheme based on the proton's arrival time at the detector was applied. After subtracting the background, the raw images were inverted using the pBasex algorithm [33] providing energy spectra and angular distributions.

We performed two calculations to get a better understanding of the experimental findings. First, in order to analyze the dependence of the results on the pulse duration, we solved the TDSE to second order of the perturbation theory [34] for pulses up to 40 fs (total duration). The use of this methodology is justified, as for the short wavelengths and peak intensities used in the experiment we are clearly in the perturbative regime. Second, we performed calculations in the infinite-time limit (i.e., the high-resolution regime where the vibronic states are resolved) by using the fully quantum-mechanical formalism of Refs. [35,36]. In both cases, we computed electronic and vibrational

(dissociative) wave functions, as well as the corresponding Hamiltonian and dipole transition matrix elements, in full dimensionality by using a basis of B-spline functions [37]. The studied transition, dominated by a two-photon process via the $B^1\Sigma_u^+$ state, is most favorable for molecules oriented parallel to the polarization direction, subsequently leading to ionization into the $^1\Sigma_g^+$ continuum. We thus restricted the calculations to this orientation, i.e., states of $^1\Sigma_{g/u}^+$ symmetries.

The measured DI/NDI ratios for resonant two-photon ionization via the $v = 8$–12 vibrational levels of the H_2 ($B^1\Sigma_u^+$) state, extracted consistently from both the photoelectron spectra and the ion TOF, are displayed in Fig. 2. Values around unity are derived, corresponding to an enhancement of almost 2 orders of magnitude compared to one-photon ionization for similar total excitation energies. The DI/NDI ratio shows a general rising trend with increasing vibrational levels for $v = 8$–11. The deviation from this tendency for $v = 12$ in the experiment is due to the occurrence of simultaneous quasiresonant excitation of the close-lying H_2 ($C^1\Pi_u$, $v = 2$) intermediate state, as proven by the ion fragment angular distribution (not shown). The corresponding computed DI/NDI ratios reported for the infinite-time limit calculations confirm the measured magnitude and the increasing trend for higher vibrational levels. This result thus demonstrates an efficient control of DI versus NDI taking advantage of the nuclear DOF in the intermediate state through the selection of the degree of vibrational excitation.

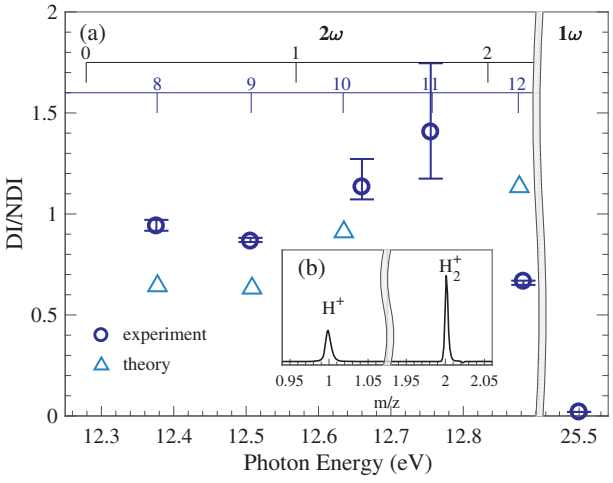

FIG. 2. (a) Experimental and theoretical DI/NDI ratio as a function of the photon energy showing a major enhancement of DI for two-photon ionization compared to the one-photon case recorded at 25.5 eV (DI/NDI ≈ 0.02) [8]. The measured ratio is derived from the PES. Error bars indicate the ratios obtained by shifting the integration limits by ±100 meV. The blue (black) comb indicates the position of the vibrational levels of the $B^1\Sigma_u^+$ ($C^1\Pi_u$) state. The computed DI/NDI ratio for $v = 11$ amounts to 3.25. Inset (b) shows the TOF mass spectrum for a FEL photon energy of 12.76 eV.

The primary observable consists of the photoelectron spectrum (PES), as featured in Fig. 3 for excitation of the H_2 ($B^1\Sigma_u^+$, $v = 9$) state at $h\nu = 12.51$ eV. Simple considerations based on energy conservation for the two-photon process set the boundaries for electron energies assigned to NDI ($2h\nu - E_D \le E_e \le 2h\nu - \mathrm{IP}$) and DI ($E_e \le 2h\nu - E_D$), respectively, where IP is the H_2 ionization potential (15.43 eV) and E_D is the position of the $H^+ + H(1s)$ dissociative ionization limit (18.08 eV). The measured PES in Fig. 3(a) displays indeed a well-resolved dip at $E_e = 6.94$ eV, separating lower and higher energies consistent with the DI-NDI limit. Although the vibrational distribution of the $H_2^+(X^2\Sigma_g^+, v^+)$ bound state reflected by the NDI structure is not resolved in the present conditions, the two-photon PES clearly favors population of high vibrational levels ($v^+ \ge 7$) with a maximum centered around $v^+ = 11$. This is in clear contrast to one-photon

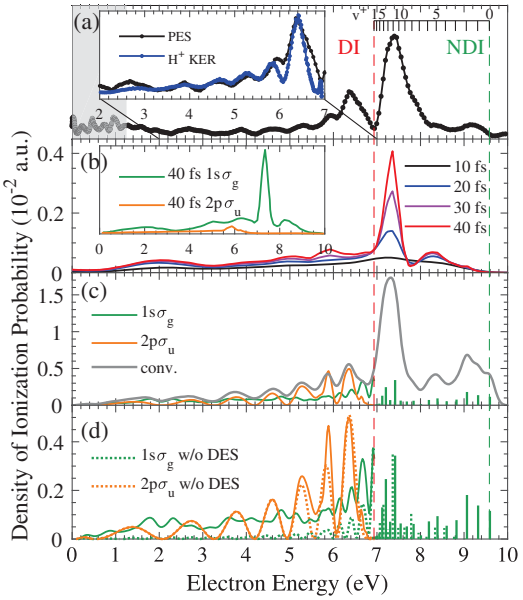

FIG. 3. (a) Experimental PES for resonant two-photon ionization via the $B(v = 9)$ state at 12.51 eV. The top-right comb features the position of the $H_2^+(X^2\Sigma_g^+, v^+)$ vibrational levels. Low-energy electrons (gray shaded area) corresponding to ionization of the intermediate state by one seed laser photon are left out in the determination of the DI/NDI ratio. The inset shows an enlargement of the DI region of the PES together with the H^+ KER spectrum. The KER scale was converted into the electron energy scale: $E_e = 2h\nu - E_D - \mathrm{KER}$. (b) Computed PES for pulse total durations $T = 10$–40 fs (normalized by T). The contributions of the two ionization continua for 40-fs pulses are illustrated in the inset. (c) Infinite-time limit spectrum. The gray line depicts a convolution of the theoretical data with a Gaussian function of FWHM = 150 meV (200 meV) for the DI (NDI) part of the spectrum to account for the experimental resolution. (d) Comparison of the infinite-time limit spectra obtained from the complete calculation (full lines) with a truncated computation in which DES are omitted (dotted lines).

ionization from the H_2 ($X^1\Sigma_g^+$, $v=0$) ground state, for which only low vibrational levels of the $H_2^+(X^2\Sigma_g^+, v^+)$ manifold are populated (maximum at $v^+=2$) [38]. This result is a first indication that the two-photon process favors ionization of the intermediate state at large internuclear distances reaching thereby high vibrational levels in the ion. The energy region assigned to DI displays oscillations, well resolved in the 3–7 eV range, characterized by an increasing intensity and a decreasing energy spacing. These oscillations are clearly mirrored in the H^+ kinetic energy release (KER) spectrum as illustrated in the inset in Fig. 3(a), reflecting energy conservation $2h\nu = E_D + E_e +$ KER, where $\mathrm{KER} = E_H + E_{H+}$. They match rather well the FC overlap of the vibrational wave function of the H_2 ($B^1\Sigma_u^+$, $v=9$) state with the $H_2^+(2p\sigma_u{}^2\Sigma_u^+)$ repulsive state, as illustrated in Fig. 1(b), close to the prediction of the Condon-reflection approximation [39,40]. The DI spectra therefore also demonstrate a strong contribution from the H_2 ($B^1\Sigma_u^+$, $v=9$) state at large R distances populating the $H_2^+(2p\sigma_u{}^2\Sigma_u^+)$ ionization continuum. Processes requiring absorption of a third photon within the VUV pulse, such as sequential dissociation of the $H_2^+(X^2\Sigma_g^+)$ bound state or ionization of $H(n)$ atoms produced by ND of the DES, are unobserved here. The two spectral regions discussed above are therefore assigned to DI and NDI, respectively, and integration leads to a DI/NDI ratio of 0.87, consistent with the one derived from the TOF spectrum.

Figure 3 provides a comparison of the experimental findings with the calculations for 10–40 fs pulse durations (b) and with those obtained in the infinite-time limit (c),(d). Consistent with previous TDSE calculations [9–11], the 10-fs-computed PES in Fig. 3(b) shows that the vibrational distribution for NDI extends to higher v^+ levels of the $H_2^+(X)$ state than found for shorter 5-fs pulses and that the KER distribution reflected in the DI component of the PES displays broad structures, emphasizing the role of autoionization of Q_1 ($^1\Sigma_g^+$) DES into the $H_2^+(X^2\Sigma_g^+)$ ionic state. For these short pulses, the strong increase of the ionization probability [9–11,41] and the DI/NDI ratio [9–11] is also due to nuclear dynamics, but such dynamics is operative only in a limited range of R distances.

Interestingly, the present experimental PES and KER spectra [Fig. 3(a)] show that, contrary to what one might infer by varying the pulse duration from 2 to 10 fs (as in Refs. [9,10]), the infinite-time limit is reached for pulses much longer than 10 fs. The time-dependent calculations [Fig. 3(b)] indeed account for an important variation of the PES for 10–40 fs pulses. Although the agreement with the measured PES improves when the pulse duration is increased, the simulations do not yet reproduce the experiment even for 40-fs pulses, a duration approaching the vibrational period for $v=9$. In particular, for DI the nascent population of the $H_2^+(2p\sigma_u{}^2\Sigma_u^+)$ repulsive state is still very weak, as illustrated in the inset in Fig. 3(b), and the broad peaks assigned to autoionization of the $Q_1(^1\Sigma_g^+)$ DES into the $H_2^+(1s\sigma_g{}^2\Sigma_g^+)$ state [11] do not match the experiment.

The agreement improves significantly when considering the infinite pulse duration calculation. Here, the DI spectrum in Fig. 3(c) nicely reproduces the observed oscillations, confirming the importance of DI into the $2p\sigma_u$ continuum, superimposed on a weakly structured component of comparable weight corresponding to ionization into the $1s\sigma_g$ continuum. The NDI part of the spectrum also shows a reasonable agreement with the experiment after convoluting computed ionization probabilities with the instrumental width, providing the density of the ionization probability. The vibrational distribution in the $H_2^+(X^2\Sigma_g^+, v^+)$ ionic state favors the $v^+=11$ level with two additional peaks around $v^+=5$ and $v^+=2$. We observe that the structure peaking at $v^+=2$, not predicted by the calculation for a 40-fs pulse, is larger than that found in the measured PES, suggesting that the experiment does not fully match the stationary conditions. A similar conclusion can be drawn when comparing the computed DI/NDI ratios for $v=9$, which vary from 1.5 to 1.2 for 10–40 fs pulses and reach 0.63 for the infinite-time limit, with the measured value 0.85. Hereby, the experiment points to a characteristic timescale lying between those for ultrafast dynamical processes and steady state excitations. In order to probe the contribution of DES with the increasing pulse duration, we compare in Fig. 3(d) the PES in Fig. 3(c) with the one obtained for a truncated computation, in which the autoionizing DES are suppressed. It shows that the contribution of DES affects DI as well as NDI mainly for the $H_2^+(1s\sigma_g{}^2\Sigma_g^+)$ continuum, the DI/NDI ratio remaining comparable.

When the vibrational level of the $B^1\Sigma_u^+$ state is varied, clear trends are observed in the PES as shown in Fig. 4. For NDI, increasing the vibrational levels leads to the

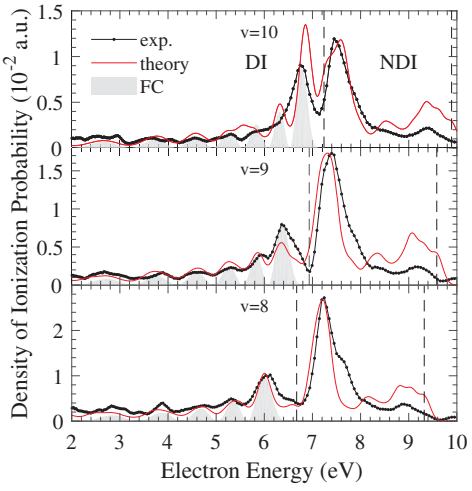

FIG. 4. Experimental and theoretical photoelectron spectra for $B^1\Sigma_u^+$ ($v=8$–10). The gray shaded areas depict the FC overlap between the $B(v)$ state with the $H_2^+(2p\sigma_u{}^2\Sigma_u^+)$ continuum.

population of higher $H_2^+(X^2\Sigma_g^+, v^+)$ levels up to the dissociation limit, while for DI it corresponds to an enhanced contribution of energetic electrons or low-energy protons. The latter can be explained by the high ionization probability near the outer-turning point of the intermediate-state vibrational wave functions, which expands from 2.7 to 3.2 Å for $v = 8$–12. Whereas the measured DI spectrum remains close to the FC overlap of the H_2 $(B^1\Sigma_u^+)$ vibrational wave function with the $2p\sigma_u$ ionic state, the computed spectrum deviates from this distribution close to the DI-NDI limit, as shown in Fig. 4. This deviation as well as the stronger ionization probability into low v^+ for NDI resulting from the calculations is attributed to autoionization into the $H_2^+(X^2\Sigma_g^+)$ continuum [cf. Fig. 3(d)], which plays a more important role in the infinite-time limit calculation than in the experiment on the 100 fs timescale.

In conclusion, exploiting the unique narrow bandwidth and tunability at FERMI in a VUV range unexplored to date with FELs, we have demonstrated a remarkable enhancement of the ratio between the dissociative and nondissociative ionization processes in resonant two-photon ionization of the H_2 molecule compared to one-photon ionization. This increase by about 2 orders of magnitude results in DI probabilities even larger than those for NDI at certain excitation energies, which is a remarkable finding for single photoionization of small molecules. This is assigned to the role of the nuclear DOF in the $B^1\Sigma_u^+$ intermediate state controlled by a selective excitation of single vibrational levels.

The recorded PES and KER spectra demonstrate that NDI favors the excitation of high v^+ levels of the $H_2^+(X^2\Sigma_g^+, v^+)$ manifold, while ionization of the $B^1\Sigma_u^+$ state into the repulsive $H_2^+(^2\Sigma_u^+)$ state dominates in DI. They emphasize the major electronic channels contributing to ionization of the $B^1\Sigma_u^+$ state at large internuclear distances, providing insight into the coupling between electronic and nuclear motion. *Ab initio* time-dependent simulations for 10–40 fs pulses and calculations in the infinite-time limit support the unambiguous identification of the DI and NDI channels and their dependence on the pulse duration.

This comparative study also suggests that using 100-fs pulses probes a timescale at the transition between ultrafast dynamics and steady state excitations. Such VUV pulses are most appropriate to investigate the role of the vibrational DOF in neutral molecules and thereby to control the outcome of nonlinear resonant photoionization processes. Future studies will extend the investigation of the role of nuclear DOF to resonant excitation of electronic states of different symmetries in H_2. Finally, similar control strategies in other diatomic or small polyatomic molecules should also be viable employing narrow-band intense VUV FEL pulses.

This research was supported by "Investissements d'Avenir" LabEx PALM (ANR-10-LABX-0039-PALM) and EquipEx ATTOLAB (ANR-11-EQPX-0005-ATTOLAB), as well as by the EU-H2020 Laserlab-Europe 654148. This work is supported by the ERC advanced Grant No. 290853—XCHEM—within the seventh framework program of the European Union. We also acknowledge the financial support from the MINECO Project No. FIS2016-77889-R and the European COST Action XLIC CM1204 and the computer time from the CCC-UAM and Marenostrum Supercomputer. A. P. acknowledges a Ramón y Cajal contract from the Ministerio de Economía y Competitividad (Spain). F. M. acknowledges support from the "Severo Ochoa" Program for Centres of Excellence in R&D (MINECO, Grant No. SEV-2016-0686) and the "María de Maeztu" Program for Units of Excellence in R&D (MDM-2014-0377). D. D. and M. H. acknowledge support by Institut de Physique (CNRS). M. M. acknowledges support by the Deutsche Forschungsgemeinschaft (DFG) under Grants No. SFB925/A3 and CUI, No. DFG-EXC1074. We gratefully acknowledge the members of the FERMI team at Elettra-Sincrotrone Trieste whose work made this experiment possible.

[*] fabian.holzmeier@u-psud.fr
[†] Present address: Lawrence Berkeley National Laboratory, Chemical Sciences, Berkeley, California 94720, USA.
[‡] Present address: LIDYL, CEA, CNRS, Université Paris-Saclay, CEA-Saclay, 91191 Gif sur Yvette, France.
[§] Present address: Université Lille, CNRS, UMR 8523—PhLAM—Physique des Lasers Atomes et Molécules, 59000 Lille, France.

[1] M. Nisoli, P. Decleva, F. Calegari, A. Palacios, and F. Martín, Chem. Rev. **117**, 10760 (2017).
[2] F. Calegari *et al.*, Science **346**, 336 (2014).
[3] A. Marciniak *et al.*, Nat. Commun. **6**, 7909 (2015).
[4] H. Ibrahim, C. Lefebvre, A. D. Bandrauk, A. Staudte, and F. Légaré, J. Phys. B **51**, 042002 (2018).
[5] Y. H. Jiang *et al.*, Phys. Rev. Lett. **102**, 123002 (2009).
[6] W. Siu *et al.*, Phys. Rev. A **84**, 063412 (2011).
[7] Y. H. Jiang *et al.*, Phys. Rev. Lett. **105**, 263002 (2010).
[8] J. W. Gallagher, C. E. Brion, J. A. R. Samson, and P. W. Langhoff, J. Phys. Chem. Ref. Data **17**, 9 (1988).
[9] A. Palacios, H. Bachau, and F. Martín, Phys. Rev. Lett. **96**, 143001 (2006).
[10] A. Palacios, H. Bachau, and F. Martín, Phys. Rev. A **75**, 013408 (2007).
[11] J. F. Pérez-Torres, J. L. Sanz-Vicario, H. Bachau, and F. Martín, J. Phys. B **43**, 015204 (2010).
[12] J. L. Sanz-Vicario, H. Bachau, and F. Martín, Phys. Rev. A **73**, 033410 (2006).
[13] E. Allaria *et al.*, Nat. Photonics **6**, 699 (2012).
[14] P. Finetti *et al.*, Phys. Rev. X **7**, 021043 (2017).
[15] R. Ma *et al.*, J. Phys. B **46**, 164018 (2013).
[16] T. Sato *et al.*, J. Phys. B **44**, 161001 (2011).
[17] M. Žitnik *et al.*, Phys. Rev. Lett. **113**, 193201 (2014).
[18] T. Mazza *et al.*, Nat. Commun. **6**, 6799 (2015).
[19] A. Dubrouil *et al.*, J. Phys. B **48**, 204005 (2015).

[20] M. Ilchen *et al.*, Phys. Rev. Lett. **118**, 013002 (2017).
[21] Y. H. Jiang *et al.*, Phys. Rev. A **81**, 021401 (2010).
[22] N. Berrah, Phys. Scr. **T169**, 014001 (2016).
[23] J. Philip, J. P. Sprengers, T. Pielage, C. A. de Lange, W. Ubachs, and E. Reinhold, Can. J. Chem. **82**, 713 (2004).
[24] C. R. Scheper, W. J. Buma, C. A. de Lange, and W. J. van der Zande, J. Chem. Phys. **109**, 8319 (1998).
[25] J. W. J. Verschuur and H. B. Van Linden Van Den Heuvell, Chem. Phys. **129**, 1 (1989).
[26] F. Aguirre and S. T. Pratt, J. Chem. Phys. **121**, 9855 (2004).
[27] C. Jungen and S. C. Ross, Phys. Rev. A **55**, R2503 (1997).
[28] H. Rottke, J. Ludwig, and W. Sandner, J. Phys. B **30**, 4049 (1997).
[29] K. Hoshina, A. Hishikawa, K. Kato, T. Sako, K. Yamanouchi, E. J. Takahashi, Y. Nabekawa, and K. Midorikawa, J. Phys. B **39**, 813 (2006).
[30] V. Lyamayev *et al.*, J. Phys. B **46**, 164007 (2013).
[31] C. Svetina *et al.*, J. Synchrotron Radiat. **22**, 538 (2015).
[32] E. Allaria *et al.*, New J. Phys. **14**, 113009 (2012).
[33] G. A. Garcia, L. Nahon, and I. Powis, Rev. Sci. Instrum. **75**, 4989 (2004).
[34] A. Palacios, J. L. Sanz-Vicario, and F. Martín, J. Phys. B **48**, 242001 (2015).
[35] A. T. Georges and P. Lambropoulos, in *Advances in Electronics and Electron Physics*, edited by L. Marton and C. Marton (Academic, New York, 1980).
[36] P. Lambropoulos, Adv. At. Mol. Phys. **12**, 87 (1976).
[37] H. Bachau, E. Cormier, P. Decleva, J. E. Hansen, and F. Martín, Rep. Prog. Phys. **64**, 1815 (2001).
[38] J. E. Pollard, D. J. Trevor, J. E. Reutt, Y. T. Lee, and D. A. Shirley, J. Chem. Phys. **77**, 34 (1982).
[39] H. D. Hagstrum, Rev. Mod. Phys. **23**, 185 (1951).
[40] B. L. G. Bakker, D. H. Parker, and W. J. van der Zande, Phys. Rev. Lett. **86**, 3272 (2001).
[41] J. Förster, Y. V. Vanne, and A. Saenz, Phys. Rev. A **90**, 053424 (2014).